

---

# Quantitative Effectiveness Assessment and Role Categorization of Individual Units in Convolutional Neural Networks

---

Yang Zhao<sup>1</sup> Hao Zhang<sup>1</sup>

## Abstract

Identifying the roles of individual units is critical for understanding the mechanism of convolutional neural networks (CNNs). However, it is challenging to give the fully automatic and quantitative measures for effectiveness assessment of individual units in CNN. To this end, we propose a novel method for quantitatively clarifying the status and usefulness of single unit of CNN in image classification tasks. The technical substance of our method is ranking the importance of unit for each class in classification based on calculation of specifically defined entropy using algebraic topological tools. It could be implemented totally by machine without any human intervention. Some interesting phenomena including certain kind of phase transition are observed via the evolution of accuracy and loss of network in the successive ablation process of units. All of the network units are divided into four categories according to their performance on training and testing data. The role categorization is excellent starting point for network construction and simplification. The diverse utility and contribution to the network generalization of units in classification tasks are thoroughly illustrated by extensive experiments on network (VGG) and dataset (ImageNet) with considerable scale. It is easy for our method to have extensional applications on other network models and tasks without essential difficulties.

measure for its importance, especially the generalization capability. Typical works (Zeiler & Fergus, 2014; Zhou et al., 2014; Mahendran & Vedaldi, 2015; Simonyan et al., 2013; Bach et al., 2015; Fong & Vedaldi, 2017) search for the image patches that maximize the score of a given unit. Instead of searching, (Nguyen et al., 2016; Dosovitskiy & Brox, 2016) artificially generate images being important for a given unit. A big attraction of the above approaches is human-interpretable, somehow providing a sense of the unit importance, but unduly intuitive and inaccurate. Also, Bau et al. (2017; 2018a; 2020) measure the degree of conceptual alignment between units and human-visual concepts (Mountain, River, etc.) predicted by another vision segmentation model. These works achieve many nontrivial contributions, such as spontaneous emergence of object detection in a scene classification (Zhou et al., 2014), and using interpretations of units to intervene networks (Bau et al., 2020). However, they don't give the complete human-free solution for the performance assessment of individual units on the specific class (images with the same label) in dataset.

Another related research trace lies in the field of network compression. Their works generally involve some rough approaches for selecting less important units, such as the Average Percentage of Zeros (APoZ) of units (He et al., 2017), L1-norm of the units (Li et al., 2016), some sparse-based methods (Li et al., 2019; Yoon & Hwang, 2017), and so on. Moreover, (Morcos et al., 2018) introduce the class selectivity from neuroscience to score the overall importance of each unit, on the basis of calculating the mean feature maps. (Alain & Bengio, 2016) propose linear classifier probe, where they report the degree of linear classification of feature maps in intermediate layers could somehow characterize the importance unit. Nevertheless, All of these works still fail to give fine-grained assessments on the degree of the importance of a certain unit to a given class.

Why directly assessing the importance of units in CNN is so tough? A key trouble here is that our understanding towards the underlying rules of feature extraction is still elusive. Almost all the previous analysis of network units focus on the overall amplitude response of convolutional operations, and big or small items in the obtained feature maps are simply chosen as the indicator of its importance based on the idea of matched filtering. Obviously, it is

## 1. Introduction

Despite the powerful learning and representation ability of convolutional neural networks (CNNs) in image classification tasks, the status and usefulness of individual network units still remain vague for lacking in effective quantitative

---

<sup>1</sup>Department of Electronic Engineering, Tsinghua University, Beijing, China. Correspondence to: Hao Zhang <haozhang@mails.tsinghua.edu.cn>.

biased for the missing of deep investigation on the change of fine intrinsic spatial structure of input image before and after convolution. In other words, some new apparatus must be invented to transform the structural variation of images in a specified class, caused by convolution with a given unit, to some quantitative index for further importance assessment. This is just the motivation for our research.

We notice that for images in a certain class to be processed by unit convolution, if the unit is important, then the output feature maps might present some highly organized patterns rather than purely random distributed ways. In other words, the degree of chaos of input images could be largely reduced by convolution with the "important" unit. Therefore, the quantitative evaluation of unit effectiveness with respect to a class may probably be done by measuring the change of degree of chaos of images in that class during the convolution operation. This could naturally lead to topological approaches. Because knowledge of topological data analysis, such as barcodes (Ghrist, 2008) and clique topology (Giusti et al., 2015), provide valuable tools to resolve the inner patterns in raw data. Also, topological techniques have gradually shown the application potential in deep learning field. (Naitzat et al., 2020) demonstrates the superiority of using ReLu activation by studying the changes in Betti numbers of a two-class neural network. Using barcode, (Gabrielsson & Carlsson, 2019) gives the topological structural changes during training that correlates to the generalization on testing data. (Rieck et al., 2018) proposes neural persistence, a topological complexity measure of network structure that could give a criterion on early stopping. (Guss & Salakhutdinov, 2018) empirically investigates the connection between neural network expressivity and the complexity of dataset by topological analysis. In (Hofer et al., 2017), topological signatures of data are evaluated and used to improve the classification of shapes.

With the help of the topological tools, we propose a novel method for quantitatively clarifying the status and usefulness of a single unit of CNN in image classification tasks. Our method consists of two parts:

- For preparation, several key concepts, including feature topology, birth point and feature entropy, are proposed. The feature topology of a feature map shares the merit of shift and scale invariance with convolution operation. The algorithm for calculations of feature entropy is also synchronized.
- Evaluate the degree of importance of individual units with respect to given input class using the feature entropy-based metric. Then all of the units could be organized in various ways, just like ranking and categorization, for the sake of network manipulation and optimization.

Finally, extensive experiments are conducted on networks (VGG) and dataset (ImageNet) with considerable scale to make our results more persuasive.

## 2. Method

Consider the convolution layer in CNN. For effective feature extraction, convolution actuates the emergence of significant components in the output feature map when local patches in input images are highly correlated to the units. More importantly, rather than purely noise image, the latent dependence hidden among pixels in an input image inhibits certain spatial organizations of these significant components. As images with the same label typically share similar features, the locations of these significant components in their convolutional output feature map exhibit analogous topological structures. Our investigation begins with unveiling this mysterious structure of feature maps.

### 2.1. Feature Topology

For input image  $\{I(x, y)\}$  to be processed by convolution operation with a certain unit  $U$  in CNN, we have feature map  $\{F(x, y, U)\}$  as the result of convolution.

$$F(x, y, U) = \sigma(I(x, y) * U(m, n) + b) \quad (1)$$

where  $*$  denotes the convolution operation,  $b$  represents the bias,  $\sigma(\cdot)$  is the activation function.

We introduce *feature topology* for  $\{F(x, y, U)\}$ , which symbolizes the spatial structure of its significant components. Define the  $v$ th-order top set  $\mathbb{T}(F, v, U)$  in feature map  $F$  as,

$$\mathbb{T}(F, v, U) = \{(x, y) \mid |F(x, y, U)| \geq t_v\} \quad (2)$$

where  $t_v$  is the  $v$ th value in the descending ordering of set  $\{|F(x, y, U)|\}$ .

Therefore the definition of feature topology emerges naturally.

**Definition 1.** *The feature topology  $\tau(F, v, U)$  of feature map  $F$  and order  $v$  is defined as the simplicial complex create by top set  $\mathbb{T}(F, v, U)$  using the method in (Giusti et al., 2015).*

Being the representations of matched features, top set is a low-level abstraction of how the features distribute in the image. Feature topology carries the topological information of top set. So it is high-level abstraction of feature distribution. It should be emphasized that as the outcome of convolution, the top set  $\mathbb{T}(F, v, U)$  and feature topology  $\tau(F, v, U)$  all depend on the unit  $U$ . Fig. 1 examples a top set and corresponding feature topology. The top set consists of the 4 points. Its feature topology  $\tau(F, 4, U)$  includes five vertices and four lines but no faces or "holes".

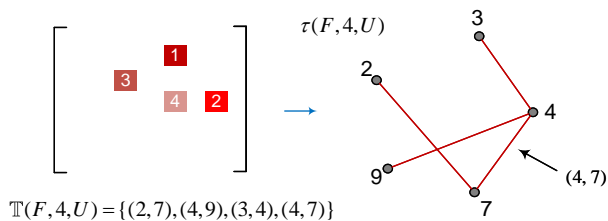


Figure 1. Example of Top Set and Feature Topology

## 2.2. Birth Point

Considering an image class  $C$  in input dataset, which is composed of the images in the same category. Losing no generality, assume cardinal of  $C$  is finite. Denote the  $i$ th image in  $C$  as  $\{I_C^{(i)}(x, y)\}$  and its feature map after convolution with unit  $U$  as  $\{F_C^{(i)}(x, y, U)\}$ . For given  $v$ , we have corresponding  $v$ th order top set  $\mathbb{T}_C(i, v, U)$  and feature topology  $\tau_C(i, v, U)$  for  $\{F_C^{(i)}(x, y, U)\}$ . Then a filtration could be created naturally

$$\tau_C(i, 1, U) \subset \tau_C(i, 2, U) \subset \dots \tau_C(i, v, U) \subset \dots \quad (3)$$

which describes the inclusion relation between feature topologies of  $\{F_C^{(i)}(x, y, U)\}$  with different  $v$ .

For each feature topology  $\tau_C(i, v, U)$  in the filtration, calculate the  $k$ th Betti numbers (Hatcher, 2002). We obtain the  $k$ th Betti curves  $\beta_C(i, v, U, k)$  for  $\tau_C(i, v, U)$ .

**Definition 2.** For  $k \geq 1$ , define birth point  $B_C(i, U, k)$  of Betti curve  $\beta_C(i, v, U, k)$  as follows ,

$$B_C(i, U, k) = \inf\{v | \beta_C(i, v, U, k) \neq 0\} \quad (4)$$

It is the minimum of the cardinal of a top set whose feature topology contain a specific "hole" structure.

We call that birth point doesn't exist if  $B_C(i, U, k) > B_C^{\max}$ . Here  $B_C^{\max}$  is a prescribed constant for practical purpose. In our experiments, it is set to be 50.

Birth point  $B_C(i, U, k)$  is a random variable essentially. In fact, we can construct a formal discrete probability space  $(\Omega, \Sigma, P)$  to describe the variety of feature maps in class  $C$ . The elements in sample space  $\Omega$  are indices of feature maps obtained by convolution operations of input images in class  $C$  with unit  $U$ .  $\Sigma$  could be set as common discrete  $\sigma$ -field and probability measure  $P$  is uniformly distributed on  $\Omega$ . In other words, Choosing an image from class  $C$  to put in convolution can be seen as a statistical experiment. Every image has an equal chance to be chosen. Afterwards,  $B_C(i, U, k)$  is defined as a random variable on  $\Omega$  (where the argument is  $i, U$  and  $k$  are parameters),

$$B_C(i, U, k) : \Omega \rightarrow \mathbb{Z} \quad (5)$$

with the probability distribution

$$P_{C,U,k}(x) = P(B_C(i, U, k) = x) = \frac{b_x}{\#(\Omega)}, \quad (6)$$

here

$$b_x = \sum_{j=1}^{\#(\Omega)} \mathbb{I}_{B_C(j, U, k)=x} \quad (7)$$

Very interesting matter could be observed from the distribution  $P_{C,U,k}(x)$ . We conjecture that the degree of concentration of  $P_{C,U,k}(x)$  gives a direct view about the performance of unit  $U$  on class  $C$  in classification tasks. More clearly, if the distribution presents a degenerate-like pattern localized at few points, the unit  $U$  is considered to be good for most information in input image is extracted by  $U$  and there is not much randomness left in feature maps; On the contrary, the distribution presents a uniform-like pattern when unit  $U$  is weak for extracting little or no information from input image and the output feature map remains almost purely random state. In a word, the degree of concentration of  $P_{C,U,k}(x)$  is supposed to be an effective indicator of the goodness of unit  $U$ .

## 2.3. Feature Entropy

To further quantize the degree of concentration of  $P_{C,U,k}(x)$ , we introduce the feature entropy  $H_{C,U,k}$ ,

$$H_{C,U,k} = - \sum_x P_{C,U,k}(x) \log P_{C,U,k}(x) \quad (8)$$

The feature-entropy-based analysis reveals some new faces of CNN training from a topological perspective. For an untrained CNN, units are initialized with random parameters. Features extracted by these units are pointless, and output feature maps are quite chaotic. It yields that the feature entropy is relatively high. Continued training could shape the units and gradually endow them with the ability to extract information to make the feature entropy decrease, that is, the output feature map more and more organized. These growth processes during training for units are diverse from each other. It naturally leads to the categories differentiation of units, which would be empirically detailed in the subsequent section.

## 3. Experiments

### 3.1. Setting

We choose the well-known ImageNet dataset and VGG16 network model to clarify our method by image classification experiments. The experiments involve four models, respectively the Keras pretrained model and three models with different generalizations that are trained by us from scratch. All four models use ReLU as their activation function. Here,

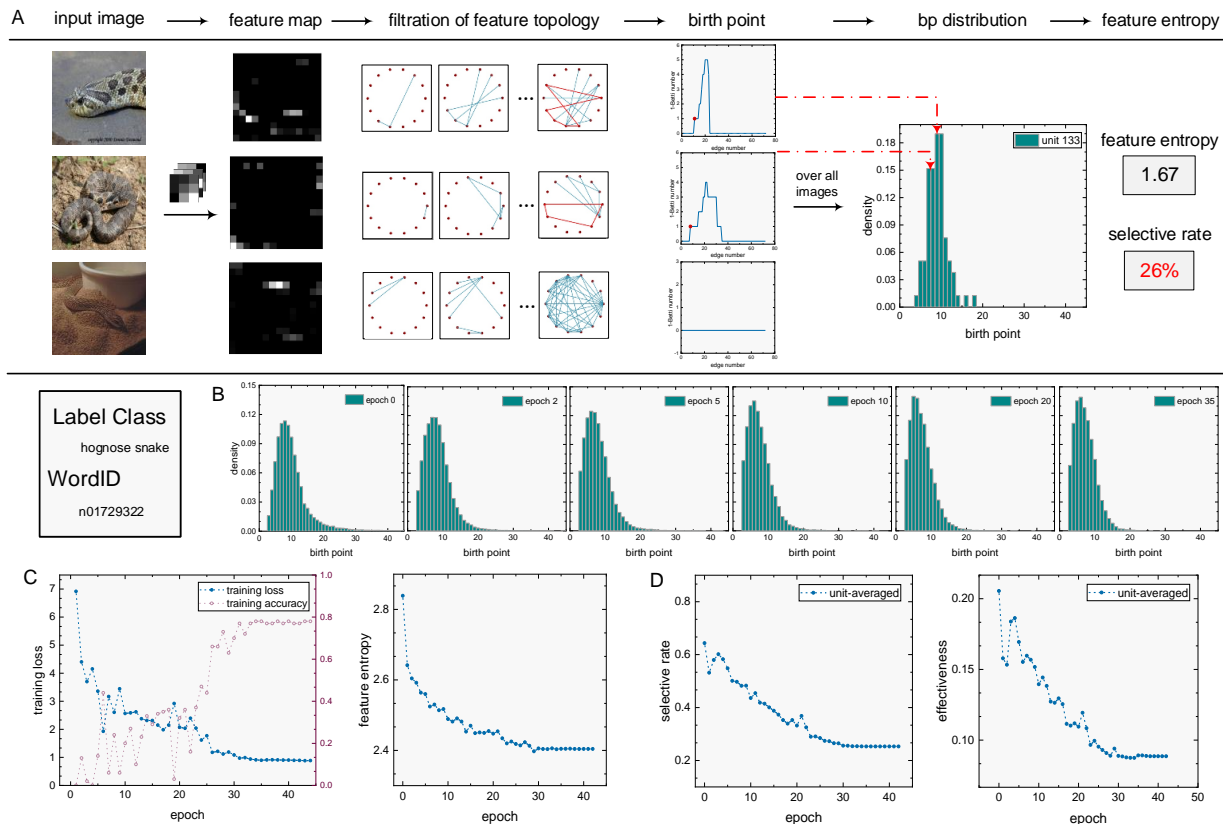


Figure 2. Calculation results of hognose snake class (wnid n01729322), on the convolution layer “conv5\_3” in VGG16. (A) Calculation flow of our method. (B) Progressive concentration of birth point distributions during training. (C) Simultaneous decrease of training loss (left) and feature entropy (right) during training. (D) Evolutions of selective rate (left) and unit effectiveness (right) during training.

we choose 512 units in the last convolution layer “conv5\_3” as our research targets of the unit effectiveness assessment. Also, we simply resize all the involved sample images to  $224 \times 224$  without implementing any data augment (like random crop) in the experiments. As the metric for network performance of image classification, we utilize both accuracy and loss for the sake of comparison.

Before the experiments, we should properly symmetrize the feature map to fit the creation of feature topologies. By preserving all the significant components, the feature map is symmetrized as

$$F_C^{(s)}(x, y, U) = \max(F_C(x, y, U), F_C^T(x, y, U)) \quad (9)$$

For clarity, We only calculate birth points  $B_C(i, U, 1)$  based on 1st betti curve for all the feature maps.

It should be noted that most of our experiments focus on *SINGLE* class (the set of images with the same label). We believe it suffices to use only the single class to reveal enough information for our purpose. Further work based on multiple classes will be done in the future.

### 3.2. Calculation Flow

In this section, we use the models trained by us to check the rule of change of feature entropy during training process. The class, which is the hognose snake (wnid n01729322) and has over 1000 images, is chosen. 100 images are randomly sampled from the class as a training set. Fig.2 A shows the calculation flow. It starts from extracting 512 feature maps from layer “conv5\_3” for each training image. Each feature map corresponds to a specific filtration of feature topology. Since the size of the feature map is  $14 \times 14$ , all the feature topologies have 14 vertices, indicating totally  $\binom{14}{2}$  elements within the filtration. Using Definition 2, we can obtain the birth point corresponding to each feature map. Next, for each unit, the distribution of birth point could be set up via Eq.6 over the 100 images in the training set. Fig.2A shows the histogram of the distribution for the unit with index 133. Therefore, The feature entropy can be calculated via Eq.8 for all the 512 units.

We claim that all of the calculation steps can be implemented fully automatically without any human intervention. Our source code will be uploaded onto github for the sake of

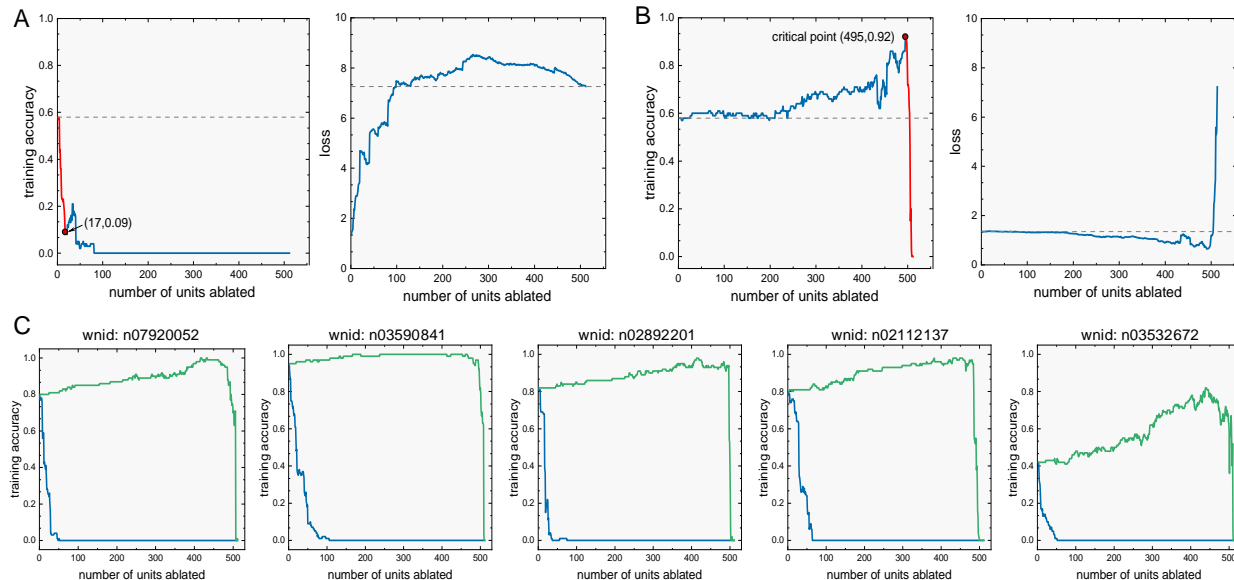


Figure 3. (A) Cumulative ablation curves of accuracy (left) and loss (right) according to the importance rank. (B) Cumulative ablation curves of accuracy (left) and loss (right) according to the the reverse order of the importance rank. (C) Cumulative ablation curves of accuracy for the classes in ImageNet according to the importance rank (blue) and its reverse order (green).

review and reuse recently.

### 3.3. Training Analysis

We investigate the variation of feature entropy while training is underway. It seems possible to track feature entropy by the index of each unit directly. However, randomness of the training optimizer (SGD) actually shuffles unit indices between epochs. So tracking by indices is meaningless. Therefore, we group the birth point distributions over all the units to present an ensemble result, as shown in Fig.2B. As expected, we could observe a clear tendency of concentration in the histograms while the epoch increases. The decrease of the feature entropy in Fig.2C(2) again confirms such tendency. By comparing with Fig.2C(1), we find that the decreasing pattern of feature entropy and that of training loss are quite similar. Both of them experience a comparable big drop in the first epoch and gradually down to the convergence point. This shows that feature entropy and training loss are both valid indicators of network performance.

Notably, the birth point in Fig. 2A(3) does not exist. Even, for unit 133, only 26% of images have birth points. The percentage of images having birth points, termed as selective rate  $\epsilon_{C,U}$  within the class  $C$  for unit  $U$ , is also a crucial factor to the effectiveness of units. Using  $\epsilon_{C,U}$ , we revise the effectiveness assessment  $E_{C,U,k}$  as,

$$E_{C,U,k} = \begin{cases} \frac{\epsilon_{C,U}}{H_{C,U,k}} & \epsilon_{C,U} \geq p \\ 0 & \epsilon_{C,U} < p \end{cases} \quad (10)$$

where  $p$  denotes the effective threshold. Here,  $p$  rules out

the particular cases that the selective rate is too low for the elements of feature maps are almost zero.

As expected, in Fig. 2D(1), we can find a clear falling of selective rate. Interestingly, the same situation in the effectiveness implies that more and more units will become unimportant for the specific class while training. Our experiments will gradually decipher the reason.

### 3.4. Ablation Test

For a more convincing demonstration, we perform our ablation test on the Keras pretrained VGG16 model. Using Eq. 10, we could give the importance rank for 512 units in layer "conv5\_3" by sorting the effectiveness of each unit in the descent order. For a given class, the ablation test (Morcos et al., 2018) checks the cumulative performance of the network by progressively inserting or removing the units according to the importance rank or its reverse order. Here, removing a unit refers to assigning outputs of the unit to all zeros.

The cumulative ablation is performed by removing units one by one according to the importance rank. Fig.3A shows the variation of the accuracy (left) and loss (right) during ablation. We can see the accuracy drops rapidly in the beginning and arrives at 0.09 after ablating only 17 units. On the other side, the loss sharply increases in the beginning just like accuracy, afterwards slowly climbing and reaching its peak value (8.53) during ablation. It should be mentioned that the peak value even exceeds that of removing all the

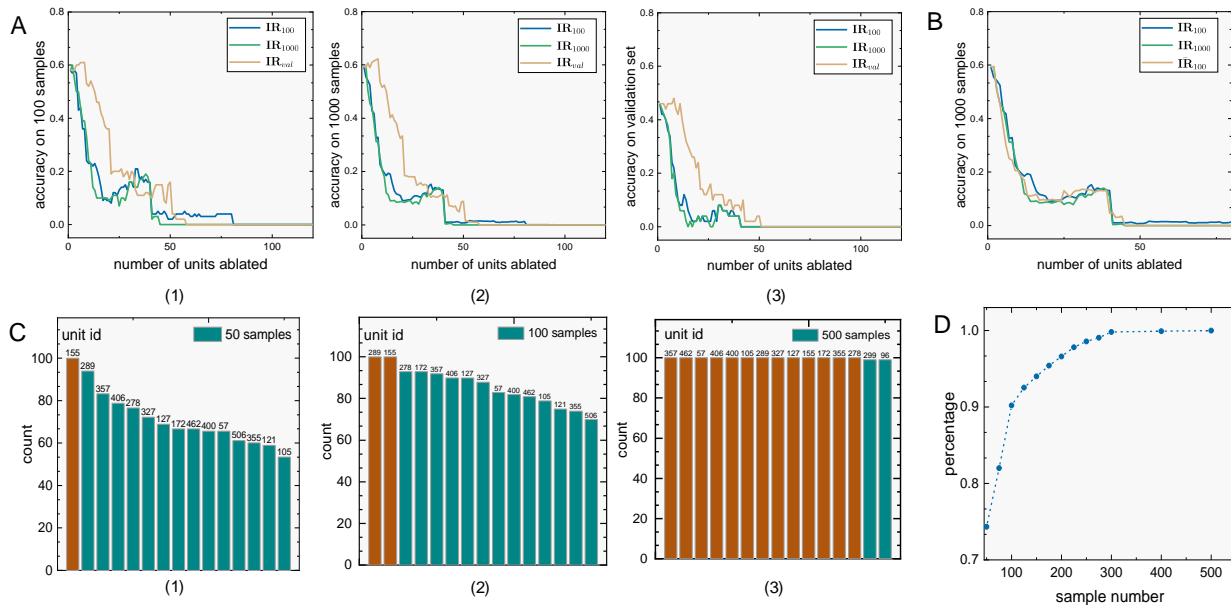


Figure 4. (A) Comparisons of cumulative ablation curves according to  $\mathbf{IR}_{100}$ ,  $\mathbf{IR}_{1000}$  and  $\mathbf{IR}_{val}$ , on  $\mathcal{S}_{100}$  (1),  $\mathcal{S}_{1000}$  (2) and  $\mathcal{S}_{val}$  (3) respectively. (B) Comparisons of cumulative ablation curves according to  $\mathbf{IR}_{100}$ ,  $\mathbf{IR}_{1000}$  and  $\overline{\mathbf{IR}}_{100}$  on  $\mathcal{S}_{1000}$ . (C) Index sets of top 15 units  $\text{IND}_K$  for 50 samples  $\text{IND}_{50}$  (1), 100 samples  $\text{IND}_{100}$  (2) and 500 samples  $\text{IND}_{500}$  (3), respectively. (D) Stability versus sample number.

units (7.26). Being somehow counterintuitive, the ablation has generated a layer even worse than all-zero layer.

We conduct cumulative ablation by removing units according to reverse importance rank to an empty layer. From Fig.3B, Instead of decreasing, the accuracy features a slow increase from 0.58 to surprising 0.92 when 96% of the units are removed. These units do not lie in the head part of importance rank and are commonly considered as the less effective units. Remarkably, starting with a certain unit is removed, the accuracy dramatically drops to zero within only 17 units. In fact, this is essentially some certain kind of phase transition phenomenon of network performance with respect to the ablation of units with the effectiveness from low to high. Additionally, the observation of loss confirms the existence of such phase transition.

To explore the universality of existence of phase transition in classes other than the chosen class, thorough ablation tests on ImageNet are done. Fig.3C shows the cumulative ablation results of some randomly sampled classes. Phase transition appears in the results of all the sampled classes.

### 3.5. Stability of Importance Rank

Does the importance rank of units keep stable with different image samples in the chosen class? To answer the question, two more sample sets are prepared except for the previous 100 samples: one includes 1000 images from the training set of ImageNet and the other one includes 50 images from

the validation set of ImageNet in the same class with 100 samples set. We use notation  $\mathcal{S}_{100}$ ,  $\mathcal{S}_{1000}$ ,  $\mathcal{S}_{val}$  for 100 samples set, 1000 samples set and the validation set, and  $\mathbf{IR}_{100}$ ,  $\mathbf{IR}_{1000}$ ,  $\mathbf{IR}_{val}$  for their corresponding importance ranks respectively.

We perform the cumulative ablation tests according to all of the three importance ranks on each sample set. The results are shown in Fig. 4A(1-3). The curves of accuracy with respect to  $\mathbf{IR}_{100}$  and  $\mathbf{IR}_{1000}$  yield nearly no difference on all the three sample sets. This demonstrates that the actual performance of two importance ranks in ablation tests are very similar. Also, the accuracy drops slower in terms of  $\mathbf{IR}_{val}$  than  $\mathbf{IR}_{100}$  and  $\mathbf{IR}_{1000}$ . It is reasonable because the pretrained network has not 'seen' the images in the validation set. Hence  $\mathcal{S}_{100}$  and  $\mathcal{S}_{1000}$  are more suitable than  $\mathcal{S}_{val}$  for pretrained network.

To test the performance fluctuation of importance rank caused by sampling difference in ablation tests, 100 different sample sets, each containing 100 images randomly selected from 1000 training images of chosen class, are constructed and grouped.  $\mathcal{G}_{100,100} = \{\mathcal{S}_{100}^{(1)}, \mathcal{S}_{100}^{(2)}, \dots, \mathcal{S}_{100}^{(100)}\}$  where the subscripts of  $\mathcal{G}$  denote the number of sets and the number of images in each set respectively. Then, we compute the mean effectiveness of units over 100 sample sets in  $\mathcal{G}_{100,100}$  by simple average to get the mean importance rank  $\overline{\mathbf{IR}}_{100}$ . As shown in Fig. 4B, we compare the ablation result on  $\mathcal{S}_{1000}$  with  $\overline{\mathbf{IR}}_{100}$ ,  $\mathbf{IR}_{100}$  and  $\mathbf{IR}_{1000}$ . Three curves

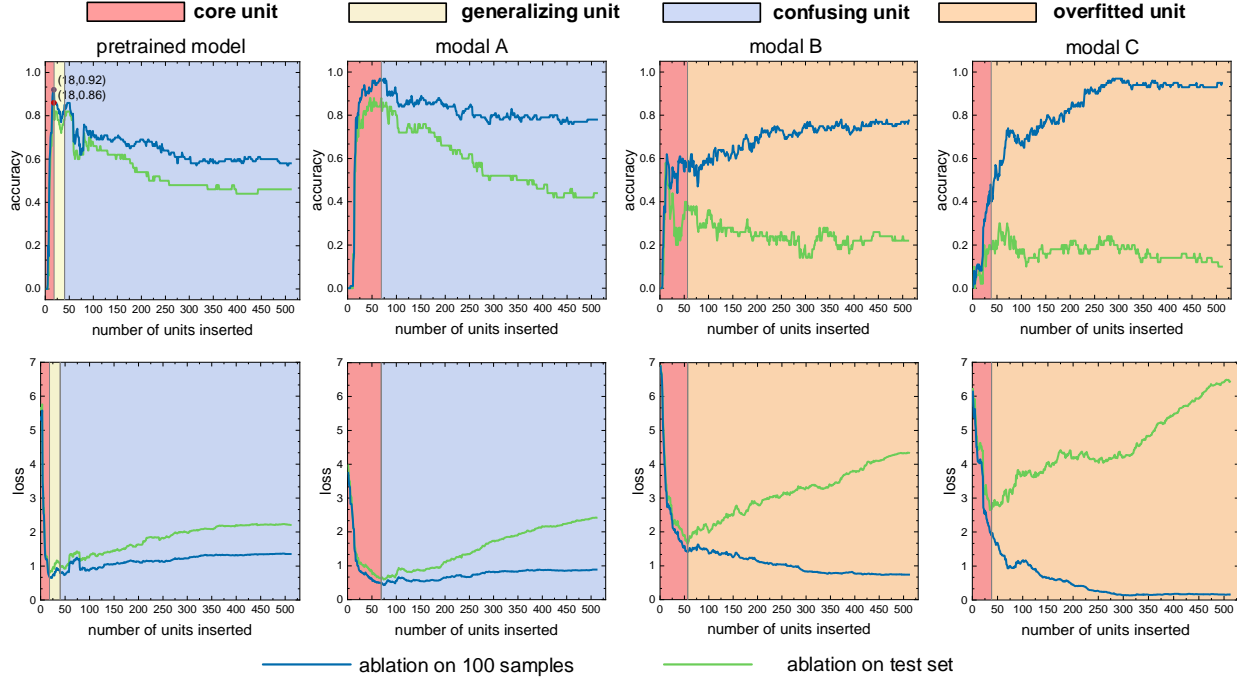


Figure 5. Role categorization for four models with different generalizations. All the units within the layer can be divided into four categories: core units (red), generalizing units (yellow), confusing units (light blue), overfitted units (orange). Reversed cumulative ablation are performed on both training set (blue curve) and test set (green curve), where accuracy (upper row) and loss (bottom row) are investigated simultaneously.

are almost the same. This indicates the importance rank is nearly independent of the selection of the sample set.

Furthermore, we check the stability of elements in importance rank, not just their performance in ablation tests. Several groups composed of sample sets with diverse sizes are constructed,  $\mathbb{G}_{100,50}, \mathbb{G}_{100,75}, \mathbb{G}_{100,100}, \dots, \mathbb{G}_{100,500}$ . For a group composed of 100 sample sets with size  $K$ , we have 100 importance ranks with descent order.

$$\mathbf{IR}_{100,K}^{(i)}, \quad i = 1, 2, \dots, 100, \quad K = 50, 75, \dots, 500 \quad (11)$$

Denote  $\mathbf{IR}_{100,K}^{(i)}(1:20)$  as the set of unit indices lying in top 20/512 of importance rank  $\mathbf{IR}_{100,K}^{(i)}$ . For unit  $j$ , we have

$$\mathbf{stat}_j^{(K)} = \sum_{i=1}^{100} \mathbb{I}_{j \in \mathbf{IR}_{100,K}^{(i)}(1:20)} \quad (12)$$

Then we sort  $\mathbf{stat}_j^{(K)}$  according to descent order,

$$\mathbf{stat}_{(1)}^{(K)} \geq \mathbf{stat}_{(2)}^{(K)} \geq \dots \geq \mathbf{stat}_{(512)}^{(K)} \quad (13)$$

Find out the index set of top 15 units  $\mathbf{IND}_K = \{(1)_K, \dots, (15)_K\}$ . The result is shown in Fig. 4C(1-3). The remarkable tendency with respect to the sample set size could be noticed. For  $\mathbb{G}_{100,500}$ , each sample set votes out

almost the same 15 units. We calculate

$$\frac{1}{10} \sum_{j=1}^{10} \frac{\mathbf{stat}_j^{(K)}}{100} \mathbb{I}_{(j)_K \in \mathbf{IR}_{1000}(1:15)}, \quad K = 50, 75, \dots, 500 \quad (14)$$

From Fig. 4D, we have the ratio (14) exceed 90% once the size of sample sets reach 100. It gives us sufficient confidence to use importance ranks obtained based on small subsets of image samples to make inferences on the ability of network units.

### 3.6. Role Categorization of Units

Based on their performance on training and test set, we find that units in a trained network model could be categorized into 4 roles: core units, overfitted units, generalizing units and confusing units. Based on the network with the same structure of VGG16, We train four models with different parameters and generalization ability to illustrate these four categories. The results are shown in Fig. 5. The previously chosen class is still utilized. For each model, we calculate the importance rank of units using 100 samples as training set. Unlike the above work, we investigate the inverse cumulative ablation on the training and the test set. It means that units are inserted into the network layer one by one according to the descent ordering of their importance.

Table 1. Classification accuracies for four different models.

MODELS	TRAINING ACC	TESTING ACC
PRETRAINED	0.58	0.46
MODEL 1	0.78	0.44
MODEL 2	0.77	0.22
MODEL 3	0.95	0.10

*Core units* are the units lying on the top of importance rank and enter the network as vanguards. They are all-rounder on both training and test sets. They are typically the cornerstone units in convolution layers for classification tasks, which is colored light red in Fig. 5. For the pretrained model (Fig. 5A), only 18 most important units suffice to promote the network performance to the peak, which is even higher than the original model. The performance declines gradually along with the addition of other units, which clearly shows the ability difference between core units and others. For model B, although 60 core units are needed for reaching performance peak, it is apparent that majority of contribution comes from 20 top units. For model C and D, which are seriously overfitted, the situation is analogous. Nevertheless, the performance on the test set deteriorates sharply when units other than core are added, no matter its continual improvement on the training set. Overfitting is visible vividly! In summary, the core units are the backbone of a network model. This thoroughly explains the performance drop by deleting certain units observed in (Zhou et al., 2018b).

*Overfitted units* are the units being good at training but bad at test sets. They come after core units in the importance rank, colored orange in Fig. 5. The performance on training keeps being improved, but its turning point appears on the test set obviously when overfitted units enter the network. Overfitted units are harmful to the network because they offset the effect of core units. The existence of overfitted units implies the continuous rising of the training performance. It is a significant sign of overfitting. Remarkably, this provides a criterion to detect overfitting using only training sets.

*Generalizing units* are the units that play well on test sets but not on training sets. Just like overfitted units, they come after core units in the important rank, colored light yellow in Fig. 5. Generalizing units are the separatrix of core units and confusing units. Normally, they are not likely to appear in the network because test sets are not involved in training. Visibility of generalizing units generally implies the model is well trained. Unfortunately, detecting these units is nearly impossible without the test set.

*Confusing units* are the units important on neither training set nor test set for this class but may be core units to other classes. They normally lie on the end part of the importance rank, colored light blue in Fig. 5. Confusing units are the products of performance balancing on diverse classes.

Opposite to the overfitted units, if we observe the continuous slight decline in the training performance along with the addition of units, the model probably might not suffers from seriously overfitting.

It is meaningful to notice that the peak performance in model B is lower than in model A. It could be intuitively explained as follows: Because lots of overfitted units excessively focus on the training set, the training on the ability of core unit is not adequate enough as model A, where the overfitted units are missing. In other words, the overfitted units compete with core units for training opportunities and hinder the normal growth of core units' ability. The competition phenomenon among the units is interesting and deserves further exploration.

Another point being worthy of remark is the training performance of pretrained model and model A exhibit somewhat slow degeneracy in pace with the participation of confusing and generalizing units. It seems that the network models 'intentionally' give up a limited part of performance on the training set to get the generalization gain on the test set in return. Maybe this kind of 'active concession' in unit behavior is the true source of intelligence in network models. It is worth deep investigating in future research.

Essentially, CNN is some kind of the art of balance. For a well-trained CNN, it should subtly control the ratio of four categories of units to reach good overall performance. Firstly, A small number of core units should be the mainstay. They decide the peak performance of the network model. Secondly, the number of overfitted units should be made as little as possible for their unacceptable performance on test sets. Their existence actually offset the gain of core units obtained. Thirdly, though being very hard, emergences of generalizing units are welcome because they are normally the indicator of good generalization. Lastly, a considerable number of confusing units should be maintained for all-round performance on all the classes in the dataset.

## 4. Conclusions

We propose a novel method that can automatically quantify the effectiveness, to a specific image class, of individual units in CNNs. Experiments show that our method could reliably give the rank of unit importance using only a small sample set for the class. According to the performance of units on training and test sets, all the units within one layer can be divided into four categories. By categorizing, the different characteristics of network units for generalization and other abilities are revealed. The status and usefulness for individual units obtained by our method provide the chance to precisely manipulate and simplify the CNNs in the future.

## References

- Alain, G. and Bengio, Y. Understanding intermediate layers using linear classifier probes. *arXiv preprint arXiv:1610.01644*, 2016.
- Bach, S., Binder, A., Montavon, G., Klauschen, F., Müller, K.-R., and Samek, W. On pixel-wise explanations for non-linear classifier decisions by layer-wise relevance propagation. *PLoS one*, 10(7):e0130140, 2015.
- Bau, D., Zhou, B., Khosla, A., Oliva, A., and Torralba, A. Network dissection: Quantifying interpretability of deep visual representations. In *Proceedings of the IEEE conference on computer vision and pattern recognition*, pp. 6541–6549, 2017.
- Bau, D., Zhu, J.-Y., Strobel, H., Lapedriza, A., Zhou, B., and Torralba, A. Understanding the role of individual units in a deep neural network. *Proceedings of the National Academy of Sciences*, 117(48):30071–30078, 2020.
- Dosovitskiy, A. and Brox, T. Inverting visual representations with convolutional networks. In *Proceedings of the IEEE conference on computer vision and pattern recognition*, pp. 4829–4837, 2016.
- Fong, R. C. and Vedaldi, A. Interpretable explanations of black boxes by meaningful perturbation. In *Proceedings of the IEEE International Conference on Computer Vision*, pp. 3429–3437, 2017.
- Gabrielsson, R. B. and Carlsson, G. Exposition and interpretation of the topology of neural networks. In *2019 18th IEEE International Conference On Machine Learning And Applications (ICMLA)*, pp. 1069–1076. IEEE, 2019.
- Ghrist, R. Barcodes: the persistent topology of data. *Bulletin of the American Mathematical Society*, 45(1):61–75, 2008.
- Giusti, C., Pastalkova, E., Curto, C., and Itskov, V. Clique topology reveals intrinsic geometric structure in neural correlations. *Proceedings of the National Academy of Sciences*, 112(44):13455–13460, 2015.
- Guss, W. H. and Salakhutdinov, R. On characterizing the capacity of neural networks using algebraic topology. *arXiv preprint arXiv:1802.04443*, 2018.
- Hatcher. *Algebraic Topology*. Cambridge University Press, London, 2002.
- He, Y., Zhang, X., and Sun, J. Channel pruning for accelerating very deep neural networks. In *Proceedings of the IEEE International Conference on Computer Vision*, pp. 1389–1397, 2017.
- Hofer, C., Kwitt, R., Niethammer, M., and Uhl, A. Deep learning with topological signatures. In *Advances in neural information processing systems*, pp. 1634–1644, 2017.
- Li, H., Kadav, A., Durdanovic, I., Samet, H., and Graf, H. P. Pruning filters for efficient convnets. In *International Conference on Learning Representations*, 2016.
- Li, Y., Lin, S., Zhang, B., Liu, J., Doermann, D., Wu, Y., Huang, F., and Ji, R. Exploiting kernel sparsity and entropy for interpretable cnn compression. In *Proceedings of the IEEE Conference on Computer Vision and Pattern Recognition*, pp. 2800–2809, 2019.
- Mahendran, A. and Vedaldi, A. Understanding deep image representations by inverting them. In *Proceedings of the IEEE conference on computer vision and pattern recognition*, pp. 5188–5196, 2015.
- Morcos, A. S., Barrett, D. G., Rabinowitz, N. C., and Botvinick, M. On the importance of single directions for generalization. In *International Conference on Learning Representations*, 2018.
- Naitzat, G., Zhitnikov, A., and Lim, L.-H. Topology of deep neural networks. *arXiv preprint arXiv:2004.06093*, 2020.
- Nguyen, A., Dosovitskiy, A., Yosinski, J., Brox, T., and Clune, J. Synthesizing the preferred inputs for neurons in neural networks via deep generator networks. *Advances in neural information processing systems*, 29:3387–3395, 2016.
- Rieck, B., Togninalli, M., Bock, C., Moor, M., Horn, M., Gumbsch, T., and Borgwardt, K. Neural persistence: A complexity measure for deep neural networks using algebraic topology. *arXiv preprint arXiv:1812.09764*, 2018.
- Simonyan, K., Vedaldi, A., and Zisserman, A. Deep inside convolutional networks: Visualising image classification models and saliency maps. *arXiv preprint arXiv:1312.6034*, 2013.
- Yoon, J. and Hwang, S. J. Combined group and exclusive sparsity for deep neural networks. In *International Conference on Machine Learning*, pp. 3958–3966, 2017.
- Zeiler, M. D. and Fergus, R. Visualizing and understanding convolutional networks. In *European conference on computer vision*, pp. 818–833. Springer, 2014.
- Zhou, B., Khosla, A., Lapedriza, A., Oliva, A., and Torralba, A. Object detectors emerge in deep scene cnns. *arXiv preprint arXiv:1412.6856*, 2014.

Zhou, B., Bau, D., Oliva, A., and Torralba, A. Interpreting deep visual representations via network dissection. *IEEE transactions on pattern analysis and machine intelligence*, 41(9):2131–2145, 2018a.

Zhou, B., Sun, Y., Bau, D., and Torralba, A. Revisiting the importance of individual units in cnns via ablation. *arXiv preprint arXiv:1806.02891*, 2018b.